Biogeosciences Discuss., 11, 9035–9069, 2014
www.biogeosciences-discuss.net/11/9035/2014/
doi:10.5194/bgd-11-9035-2014
© Author(s) 2014. CC Attribution 3.0 License.

Biogeosciences Discussions
Open Access

This discussion paper is/has been under review for the journal Biogeosciences (BG). Please refer to the corresponding final paper in BG if available.

Early season mesopelagic carbon remineralization and transfer efficiency in the naturally iron-fertilized Kerguelen area

S. H. M. Jacquet[1,2], F. Dehairs[3], A. J. Cavagna[3], F. Planchon[4], L. Monin[5], L. André[5], I. Closset[6], and D. Cardinal[6]

[1]Aix Marseille Université CNRS/INSU, IRD, Mediterranean Institute of Oceanography (MIO), UM110, 13288 Marseille, France
[2]Université de Toulon, CNRS/INSU, IRD, Mediterranean Institute of Oceanography (MIO), UM110, 83957 La Garde, France
[3]Vrije Universiteit Brussel, Analytical, Environmental & Geo-Chemistry and Earth System Sciences, Brussels, Belgium
[4]Laboratoire des Sciences de l'Environnement Marin (LEMAR), Université de Brest, CNRS, IRD, UMR6539, IUEM; Technopôle Brest Iroise, Place Nicolas Copernic, 29280 Plouzané France
[5]Royal Museum for Central Africa, Leuvensesteenweg 13, Tervuren, 3080, Belgium
[6]Sorbonne Universités (UPMC, Univ Paris 06)-CNRS-IRD-MNHN, LOCEAN Laboratory, 4 place Jussieu, 75005 Paris, France

Received: 6 May 2014 – Accepted: 12 May 2014 – Published: 16 June 2014

Correspondence to: S. H. M. Jacquet (stephanie.jacquet@mio.osupytheas.fr)

Published by Copernicus Publications on behalf of the European Geosciences Union.

CC BY

Abstract

We report on the zonal variability of mesopelagic particulate organic carbon) remineralization and deep carbon transfer potential during the Kerguelen Ocean and Plateau compared Study 2 expedition (KEOPS 2; October–November 2011) in an area of the Polar Front supporting recurrent massive blooms from natural Fe fertilization. Mesopelagic carbon remineralization was assessed using the excess, non-lithogenic particulate barium (Ba_{xs}) inventories in mesopelagic waters and compared with surface primary and export productions. Results for this early season study are compared with results obtained earlier (2005; KEOPS 1) for the same area during summer. For the Kerguelen plateau (A3 site) we observe a similar functioning of the mesopelagic ecosystem during both seasons (spring and summer), with less that 30 % of carbon exported from the upper 150 m being remineralized in the mesopelagic column (150–400 m). For deeper stations (> 2000 m) located on the margin, inside a Polar Front meander, as well as in the vicinity of the Polar Front, east of Kerguelen, remineralization in the upper 400 m in general represents > 30 % of carbon export, but when considering the upper 800 m, in some cases, the entire flux of exported carbon is remineralized. It appears that above the plateau (A3 site) mesopelagic remineralization is not a major barrier to the transfer of organic matter to the sea-floor (close to 500 m). There the efficiency of carbon sequestration into the bottom waters (> 400 m) reached up to 87 % of the carbon exported from the upper 150 m. In contrast, at the deeper locations mesopelagic remineralization clearly limits the sequestration of carbon to depths > 400 m. For sites at the margin of the plateau (station E-4W) and the Polar front (station F-L), mesopelagic remineralization even exceeds upper 150 m export, resulting in a null sequestration efficiency to depths > 800 m. In the Polar Front meander, where successive stations form a time series, the capacity of the meander to transfer carbon to depth > 800 m is highly variable (0 to 73 %). The highest carbon transfer efficiencies in the meander are furthermore coupled to intense and complete deep (> 800 m) rem-

cc BY

ineralization, resulting again in a close to zero deep (> 2000 m) carbon sequestration efficiency there.

1 Introduction

While numerous artificial (Boyd et al., 2000, 2004; Gervais et al., 2002; Buesseler et al., 2004, 2005; de Baar et al., 2005; Hoffmann et al., 2006) and natural (Blain et al., 2007; Pollard et al., 2009; Zhou et al., 2010, 2013) iron-fertilization experiments in the Southern Ocean demonstrated the role of iron in enhancing the phytoplankton biomass and production in high-nutrient low-chlorophyll (HNLC) regions, determining to what extent fertilization could modify the transfer of particulate organic carbon (POC) to the deep ocean is far from being comprehensively achieved (Morris and Charette, 2013). This is partly due to the short term over which the observations were made, precluding extrapolation to longer time scales. Moreover, when assessing whether Fe-supply could induce vertical POC transfer, the magnitude of the export from surface is not the only important parameter to take into account. Indeed, POC fate in the mesopelagic zone (defined as 100–1000 m depth layer) is often largely overlooked although these depth layers are responsible for the remineralization of most of the POC exported from the surface layer (Martin et al., 1987; Longhurst, 1995; Lampitt and Antia, 1997; François et al., 2002; Buesseler et al., 2007; Buesseler and Boyd, 2009). Only few studies considered mesopelagic C remineralization rates (Buesseler et al., 2007b; Jacquet et al., 2008a, b, 2011a, b; Salter et al., 2007) to estimate the response of deep POC export to fertilization. Assessing mesopelagic C remineralization is pivotal to evaluate remineralization length scale, the time scale of the C storage in the deep ocean, and thus to quantify the ocean's biological carbon pump and its efficiency in the global carbon (C) cycle which bears large uncertainty and is currently under debate (e.g. from 5 Gt yr^{-1} in Henson et al. (2011) to 21 Gt C yr^{-1} in Laws et al. (2000) and 13 Gt yr^{-1} in IPPC WG1 report (2013, ch. 6).

BGD
11, 9035–9069, 2014

CC BY

The present work aims at understanding the impact of a natural iron-induced bloom on the mesopelagic POC remineralization and zonal variability in the Southern Ocean. Here, C remineralization was assessed from particulate biogenic Ba (hereafter called excess-Ba or Ba_{xs}; mainly forms as barite $BaSO_4$ crystals) contents in the mesopelagic water column. The link between barite and C remineralization resides in the fact that this mineral precipitates inside oversaturated micro-environments (biogenic aggregates) during the process of prokaryotic degradation of sinking POC (Dehairs et al., 1980, 1992, 1997, 2008; Stroobants et al., 1991; Cardinal et al., 2001, 2005; Jacquet et al., 2007, 2008, 2011; Planchon et al., 2013). Once the aggregates have been remineralized, barites are released and spread over the mesopelagic layer. Overall, earlier works highlight the fact that suspended barite in mesopelagic waters builds up over the growing season and reflects integrated past remineralization activity. An algorithm relating mesopelagic Ba_{xs} contents to oxygen consumption (Shopova et al., 1995; Dehairs et al., 1997) allowed remineralization of POC fluxes to be estimated for the mesopelagic layer. Combined with surface C production and export estimates, mesopelagic Ba_{xs} also informs on the efficiency of the system toward deep carbon transfer. From earlier studies, the efficiency of C transfer through the mesopelagic layer was reported to increase under artificially induced (EIFEX; Strass et al., 2005; Smetacek et al., 2012) and natural (KEOPS; Blain et al., 2007) Fe-replete conditions (Jacquet et al., 2008a, b; Savoye et al., 2008) compared to Fe-limited, non-bloom, HNLC reference stations in the Southern Ocean. In contrast, C transfer efficiency through the mesopelagic layer was reported smaller in natural Fe-replete locations during the SAZ-Sense cruise (Jacquet et al., 2011a, b) off Tasmania. Differences in plankton community structure and composition (diatoms vs. flagellates) were pointed at, as possible causes of such discrepancies. Also, differences in integration time scales for the processes that control the carbon fluxes in artificially vs. naturally Fe fertilized systems, may yield an incomplete picture of the C transfer potential and lead to misleading conclusions. Here, we examine changes in mesopelagic POC remineralization during the early spring (October–November 2011) KEOPS 2 expedition to the Kerguelen Plateau. This same area was

BGD
11, 9035–9069, 2014

cc BY

visited earlier in 2005 during summer (KEOPS 1; January–February, 2005). This condition offers a unique opportunity to estimate the main carbon fluxes over most of the growth season.

The specific objectives of the present work are to assess the zonal variability of mesopelagic C remineralization and deep C transfer potential in the naturally iron fertilized Polar Front (PF) area eastward of Kerguelen island, and to identify possible causes inducing this variability. The rationale guiding the sampling pattern at sea was therefore to (1) examine whether or not inter-sites changes in mesopelagic carbon remineralization due to unequal surface production is a proxy for long-term temporal evolution, induced by climate change (Ridgway and Dunn, 2007) and (2) compare mesopelagic C remineralization estimates to particle and biological parameters as reported in other papers included in this issue (Cavagna et al., 2014; Dehairs et al., 2014; Jouandet et al., 2014; Laurenceau et al., 2014; Planchon et al., 2014; Trull et al., 2014; Vandermerve et al., 2014; Zhou et al., 2014).

2 Experiment and methods

2.1 Study area

The KEOPS 2 cruise (Kerguelen Ocean and Plateau compared Study; October–November 2011) was carried out in the Kerguelen Plateau area (Indian sector of the Southern Ocean) in Austral spring conditions. The northeastern part of the Plateau supports a recurrent massive bloom and the possible sources and mechanisms for fertilization were investigated during ANTARES 3 (1995; Blain et al., 2001) and the first KEOPS cruise, later referred to as KEOPS 1 (January–February 2005, late summer conditions; Blain et al., 2007, 2008). During KEOPS 2 the evolution of Chl *a* data based on multi-satellite imagery of the study area revealed the evolution of different Chl *a* rich plumes (D'ovidio et al., 2014) (Fig. 1a; e.g. Chl *a* map from 11 November 2011). The guiding hypothesis of KEOPS 2 was that the state of progress of the blooms was dif-

BGD
11, 9035–9069, 2014

ferent at each station, implying different mesoscale mechanisms responsible of their structure. Stations were sampled in distinct zones covering these different bloom patterns (Fig. 1a) (corresponding stations are reported in Fig. 1.b): (a) on the shallow plateau (station A3; see 1 in Fig. 1a). Note that station A3 coincides with a site studied during the KEOPS 1 cruise, and that it was sampled twice over a 27 day period; (b) in a meander formed by a quasi-permanent retroflection of the Polar Front (PF) and topographically-steered by the eastern escarpment (Gallieni Spur) of the Kerguelen Plateau (mainly stations E, sampled as a quasi-lagrangian temporal series) (see 2 in Fig. 1a); (c) along a North–South Transect (referred to as TNS stations; see 3, grey line in Fig. 1a) and a West–East Transect (referred to as TWE stations; see 4, grey line in Fig. 1a), both crossing the PF; and (d) in the Polar Front Zone (PFZ) in the vicinity (east) of the PF (station F-L; see 5 in Fig. 1a). Furthermore we also sampled a reference HNLC/non bloom/non Fe-fertilized station southwest of the Plateau (station R-2; see 6 in Fig. 1a). Station locations are given in Table 1.

Detailed descriptions of the complex physical structure of the area, circulation, water masses and fronts are given in Park et al. (2014). Briefly, the main hydrodynamic features observed during the cruise are the following (see θ–S diagram, Fig. 2a): (1) North of the PF, stations in the PFZ (TNS-1, TEW-8 and F-L) present Antarctic Surface Waters (AASW; $\theta \simeq 4\,^{\circ}$C and density < 27); θ–S characteristics between 150 to 400 m at station F-L (and to a lesser extent at station TNS-1) reveal the presence of interleaving with waters from northern (subantarctic) origin, centered between the 27.2 and 27.5 density curves, where Antarctic Intermediate Waters (AAIW) are usually found. This contrasts with the situation at station TEW-8, where there is no evidence of interleaving; (2) stations south of the PF exhibit subsurface temperature minima characteristic of Winter Waters (WW); below the WW three water masses can be identified, namely: the Upper (temperature maximum) and Lower (salinity maximum) Circumpolar Deep Water (UCDW and LCDW), and the Antarctic Bottom Water (AABW). Theses water masses are present roughly in the following depth intervals: 700 m < UCDW < 1500 m; 1500 m < LCDW < 2500 m; AABW > 2500 m.

CC BY

Based on the θ–S characteristics (Fig. 2a and b) and surface phytoplankton biomasses we can schematically group the stations as follows. The R-2 HNLC reference station (white dot in Fig. 1b) is characterized by a very low biomass (with low iron contents; Bowie et al., 2014). Stations TEW-3 and TNS-8 (black dots) are characterized by a low to moderate biomass and Fe contents. Stations A3 and E-4W (red dots; south of the PF) as well as stations TNS-1, F-L and TEW-8 (blue dots; north of the PF) are characterized by high biomass and iron contents. Stations in the core of the PF meander (green dots; stations TNS-6, E-1, E-2, E-3, E-4E and E-5 considered as a temporal series) are characterized by moderate biomass and iron contents.

2.2 Sampling and analyses

22 CTD casts (surface to 500–2000 m) were sampled for particulate barium (Table 1) using a CTD-rosette equipped with 22 10 L Niskin bottles. Deep particulate Ba profiles (> 1000 m) were not systematically obtained from the same CTD cast, but from successive casts sampled closeby in time and space and having similar θ–S data profiles. In the following, we use both the station and CTD numbers to refer to stations.

4 to 7 L of seawater were filtered onto 47 mm polycarbonate membranes (0.4 µm porosity) under slight overpressure supplied by filtered air (0.4 µm). The filters were rinsed with Milli-Q grade water (< 5 mL) to remove sea salt, dried (50 °C) and stored in Petri dishes for later analysis. In the home-based laboratory we performed a total digestion of samples using a tri-acid (0.5 mL HF/1.5 mL HCl/1 mL HNO_3; all Suprapur grade) mixture in closed telfon beakers overnight at 90 °C in a clean pressurized room. After evaporation close to dryness samples were re-dissolved into around 13 mL of HNO_3 2 %. The solutions were analysed for Ba and other major and minor elements by ICP-QMS (inductively coupled plasma-quadrupole mass spectrometry; X Series 2 ThermoFisher) equipped with a collision cell technology (CCT). Among all elements analysed, particular interest went to Ba and Al. The average standard error on Ba is 5 % and on Al is 8 %. The presence of sea-salt was checked by analysing Na and the sea-salt particulate Ba contribution was found negligible. Biogenic barium (hereafter

BGD
11, 9035–9069, 2014

called excess-Ba or Ba_{xs}) was calculated as the difference between total particulate Ba and lithogenic Ba using Al as the lithogenic reference element (Dymond et al., 1992; Taylor and McLennan, 1985). At most sites and depths the biogenic Ba_{xs} represented > 95 % of total particulate Ba. Lithogenic Ba reached up to 20 % of total particulate Ba at some depths in the upper 80–100 m, mainly at station R-2 and stations north of the Polar Front (i.e., TEW-8, F-L and TNS-1). The standard uncertainty (Ellison et al., 2000) on Ba_{xs} data ranges between 5 and 5.5 %. Ba_{xs} and Al data are reported in Table A1.

2.3 C remineralization

Particulate organic carbon remineralization in the mesopelagic layer (later referred to as MR) was estimated using an algorithm relating mesopelagic Ba_{xs} contents and oxygen consumption based on earlier observations in the Southern Ocean (Shopova et al., 1995; Dehairs et al., 1997, 2008). The detailed calculations are described in Jacquet et al. (2008a, 2011). Briefly, we use the following equations:

$$J_{O_2} = (Ba_{xs} - Ba_{residual})/17\,450 \tag{1}$$

$$C_{respired} = Z \times J_{O_2} \times RR \tag{2}$$

where J_{O_2} is the O_2 consumption (µmol L^{-1} d^{-1}) and $C_{respired}$ is the Mineralization Rate of organic carbon (in mmol C m^{-2} d^{-1}; MR); Ba_{xs} is the depth-weighted average Ba_{xs} value (DWAv), i.e. the Ba_{xs} inventory divided by the depth layer considered Z, $Ba_{residual}$ is the residual Ba_{xs} signal (or Ba_{xs} background) at zero oxygen consumption and RR is the Redfield C/O_2 molar ratio (127/175; Broecker et al., 1985).

DWAv Ba_{xs} values were calculated both for 150 to 400 m (Plateau and deep stations) and 150 to 800 m water column (deep stations only) (see details further below). The residual Ba_{xs} is considered as "preformed" Ba_{xs}, left-over after partial dissolution and sedimentation of Ba_{xs} produced during a previous phytoplankton growth event. In $BaSO_4$ saturated waters, such as the ones filling the whole ACC water column (Monnin et al., 1999), this background Ba_{xs} value was considered to reach 180 pM (see Dehairs et al., 1997; Jacquet et al., 2008a, 2011). Relative standard uncertainties (Ellison et al., 2000) on C remineralization ranged between 4 and 20 %.

3 Results

3.1 Particulate biogenic Ba_{xs} profiles

We focus on the mesopelagic zone where most of the remineralization of exported POC takes place (Martin et al., 1987; Sarmiento et al., 1993; Buesseler et al., 2007). Ba_{xs} profiles in the upper 800 m are reported in Fig. 3. Data for all Ba_{xs} profiles are given in Table 1A.

The Ba_{xs} profile for station R-2 (CTD #17) displays a characteristic mesopelagic Ba_{xs} maximum reaching up to 834 pM at 304 m (Fig. 3a). Ba_{xs} profiles for stations A3 on the shallow plateau (A3-1 CTD #4 and A3-2 CTD #107; Fig. 3b) have lower Ba_{xs} contents in the water column, with values ranging from about 80 to 350 pM. At this site, Ba_{xs} values increase close to the seafloor for both repeats, reaching up to 1108 pM (A3-1, 474 m) and 1842 pM (A3-2, 513 m). In contrast, station E-4W (located further north along the margin in deeper waters, but with similar θ–S and Chl *a* characteristics as station A3) displays a large mesopelagic Ba_{xs} maximum reaching up to 627 pM at 252 m (Fig. 3c). Station TEW-3 (located on the Kerguelen plateau, in waters with similar θ–S and Chl *a* characteristics as station TNS-8) has a similar profile as observed at station A3-2, except we do not observe increased Ba_{xs} contents in bottom water, as is the case for plateau sites A3-1 and A3-2 sites (Fig. 3d). The other stations of the study area (Fig. 3d–g) has a similar profile as observed at station E-4W, with Ba_{xs} contents increasing below 150 m in the mesopelagic zone and profiles showing the characteristic Ba_{xs} maxima between 200 and 500 m. Note that for most of the stations, Ba_{xs} concentrations in waters below the maximum do not systematically decrease to reach the Ba_{xs} background level (180 pM; see above). In some cases Ba_{xs} contents

BGD
11, 9035–9069, 2014

CC BY

significantly higher than residual Ba_{xs} are still observed below 1000 m (see Table 1A). This is particularly salient at stations TNS-6, E-1, E-2 and F-L where Ba_{xs} values below 1000 m reach 410 pM at 1886 m (TNS-6) and 436 pM at 1498 m (E-1).

3.2 Depth-weighted average Ba_{xs} content of mesopelagic waters

From previous studies we know that Ba_{xs} in surface waters is distributed over different mainly non-barite, biogenic phases (see Stroobants et al., 1991; Jacquet et al., 2007b; Cardinal et al., 2005). As such, they do not reflect POC remineralization processes, in contrast to mesopelagic waters where Ba_{xs} is mainly composed of barite (Dehairs et al., 1980) formed during prokaryotic degradation of sinking POC (see above). In general we observed that Ba_{xs} concentrations increase below 150 m (i.e., they increase above the background level set at 180 pM). Since the bases of the mixed layer and the euphotic zone, are both shallower than 150 m, the 150 m depth is taken here as the upper boundary of the mesopelagic domain. The depth-weighted average (DWAV) Ba_{xs} contents, calculated for the 150–400 m and 150–800 m depth intervals, are given in Table 1. For profiles on the plateau (500 m water column) bottom waters with evidence of sediment resuspension were not taken into account when calculating DWAv Ba_{xs} values (≥ 400 m). Particle size spectra indicate that sediment resuspension occurred especially at stations A3 and TEW-3 (Jouandet et al., 2014; Lasbleiz et al., 2014; Vandermerve et al., 2014; Zhou et al., 2014). Thus, at site A3 (Fig. 3b) DWAV Ba_{xs} is calculated for the layer between 150 and 354 m for A3-1 (CTD #4) and between 150 and 405 m for A3-2 (CTD#107). For station TEW-3 (CTD #38) DWAV Ba_{xs} was calculated for the water layer between 150 and 400 m (Fig. 3d). For the deep sites, we considered both, the 150–400 m and the 150–800 m depth intervals, when calculating the DWAV Ba_{xs} contents.

DWAV Ba_{xs} values range from 199 to 572 pM (Table 1) and fit within the range reported for Polar Front areas during previous studies (Cardinal et al., 2001, 2005; Jacquet et al., 2005, 2008a, b, 2011; Planchon et al., 2013). Station R-2 shows the highest DWAV Ba_{xs} of the whole study area (572 pM; 150–400 m). The 2 successive

BGD
11, 9035–9069, 2014

cc BY

visits (27 day interval) at site A3 yielded relatively low DWAV Ba_{xs} values of 267 and 316 pM, and a quite similar value was observed for shallow station TEW-3 (324 pM), located further north on the plateau. The time series stations in the Polar Front meander had DWAV Ba_{xs} contents ranging from 258 to 427 pM (150–400 m), so reaching values exceeding those on the plateau. For the time series stations, values decreased between day 0 (TNS-6) and 12 (E-3), and then increased again at days 22 (E-4E) and 27 (E-5). Stations E-4W and TNS-8 close to the Kerguelen margin, at the edge the high biomass plume (Fig. 1) had the highest DWAV Ba_{xs} values, not considering the R-2 reference station (468 and 473 pM, respectively; 150–400 m). The Polar Front F-L site, although located underneath the eastern part of the high biomass had a smaller DWAV Ba_{xs} value of 345 pM (150–400 m) and the closeby station TEW-8 even had the lowest DWAV Ba_{xs} value of the study area (199 pM; 150–400 m).

Depth weighted average Ba_{xs} values were translated into carbon remineralization rates using Eqs. (1) and (2) given above. These rates ranged from 2 to 91 mg C m^{-2} d^{-1} (Table 1).

4 Discussion

An important question relates to the fate of the exported POC: how much of this POC is respired in the mesopelagic waters and how much escapes remineralization and is exported to deeper layers where longer term sequestration is likely (see e.g. Schneider et al., 2008). To address these questions, we define two ratios: (1) the mesopelagic C remineralization efficiency (r ratio in Table 2) which is the ratio of mesopelagic C remineralization (MR, based on the DWAV Ba_{xs} concentrations) over C export (EP) from the 150 m horizon (based on ^{234}Th, see Planchon et al., 2014), and (2) the C sequestration (or transfer) efficiency at 400 and 800 m (i.e., T400, T800 in Table 2) which is the fraction of C export (EP) at 150 m passing through the 400 m (T400) or the 800 m (T800) horizons (e.g., T400 = EP400/EP150 = 1 – (MR/EP150), with MR/EP150 = r ratio; see above). This approach is similar to the one developed by Buesseler and Boyd

BGD
11, 9035–9069, 2014

(2009). Indeed, the latter authors state that a conventional curve-fitting of particle flux data (i.e., power law or exponential) skews our interpretation of the mesopelagic processes and they recommended the use of combined metrics to capture and compare differences in flux attenuation. In the following, we compare MR fluxes for the different KEOPS 2 areas (Reference site; Plateau sites; Polar Front and Polar Front Meander) and discuss remineralization and sequestration efficiencies for those sites for which primary production (PP) and/or EP data (Table 2) are available. PP data were integrated over the euphotic layer (i.e., till the 1 % PAR level; Cavagna et al., 2014), while EP fluxes are discussed by Planchon et al. (this issue). In order to compare EP with MR (*r* ratio and transfer efficiency), we considered EP fluxes from 150 m.

4.1 Reference station R-2

Because the low productivity, low export reference station R-2 had the highest DWAV Ba_{xs} content, it yields the highest MR flux of the whole study area (91 mg C m^{-2} d^{-1}; 150–800 m; Table 2). PP and EP fluxes at R-2 are both extremely low (132 and 10 mg C m^{-2} d^{-1}, respectively) and since MR exceeds EP, this results in T400 and T800 values > 100 % (Table 2). We note that the sinking flux collected using gel traps was relatively small too (Trull et al., 2014), and that the collected particles mainly consisted of phytodetrital aggregates that held heavily silicified diatoms (Laurenceau et al., 2014). Also, suspended particles in the depth range with the Ba_{xs} maximum were marked by two size fractions disappearing below 500 m depth (i.e., 3–8 µm and 12–80 µm fractions; Zhou et al., 2014). It is likely that we observe a remineralization activity that was fuelled by an important past winter production and export event. Moreover, we do note that surface waters at R-2 experienced already some significant nitrate consumption as compared to subsurface Winter Waters (T_{min} waters). Indeed, surface waters had 17 % less nitrate than Winter Water (25.7 µM at 5 m vs. 30 µM at 250 m) and the isotopic enrichment of this surface nitrate confirmed an imprint of uptake (see Dehairs et al., 2014). This would indicate that the mesopelagic Ba_{xs} content at R-2 does indeed reflect remineralization of organic material from a later winter bloom. Similarly, F. Dehairs

BGD
11, 9035–9069, 2014

CC BY

(unpublished results) observed the presence of significant numbers of barite micro-crystals in mesopelagic waters at the KERFIX time series station (50°40′ S, 68°25′ E) located east of R-2 during late winter (November 1993). Results would thus suggest the occurrence in this area of recurrent winter production and important remineralization events.

4.2 Station A3 on the plateau

The MR fluxes on the plateau vary little between the two visits 27 days apart (Table 1) and as discused below are moreover similar to KEOPS 1 summer values (see Jacquet et al., 2008a), when the same A3 site was sampled 3 times over a 19 day period. For comparison purposes, we recalculated the DWAV Ba_{xs} and MR values of KEOPS 1 by considering upper and lower mesopelagic layer boundaries of 150 and 400 m rather than 125 and 450 m, as in Jacquet et al. (2008a). Also, in the latter study the high Ba_{xs} contents observed near the seafloor were not excluded from the calculations, while they are here. These increased benthic boundary layer Ba_{xs} contents (observed also during KEOPS 2) are due to sediment resuspension which extended up to 70 m above the seafloor during KEOPS 1 (Blain et al., 2008; Venchiarutti et al., 2008; Armand et al., 2008). Because of these slightly different depth intervals over which Ba_{xs} values were integrated, the KEOPS 1 values discussed here will be slightly different from those reported in Jacquet et al. (2008a). PP and EP data from KEOPS 1 are detailed in Lefèvre et al. (2008) and Mosseri et al. (2008), and Savoye et al. (2008), respectively.

While MR fluxes at A3 ranged from 11 to 14 mg C m^{-2} d^{-1} (with a standard uncertainly around 5 %) during KEOPS 2 (spring) they were slightly larger during KEOPS 1 (summer; 17 to 23 mg C m^{-2} d^{-1}). We observe large differences in mesopelagic POC remineralization efficiency between both seasons (*r* ratio, blue values in Fig. 4, Table 2). During KEOPS 1 *r* ratios remained low, ranging from 7 to 9 % of EP at A3, while during KEOPS 2 *r* ratios decreased from 29 % (A3-1; first visit) to 13 %, 27 days later (A3-2; second visit). This variation in *r* ratio is mostly due to an increase of EP (from 47 to 85 mg C m^{-2} d^{-1}) over the same period while MR shows little change. Although at this early stage of the season (spring), PP at A3-2 already reaches 2172 mg C m^{-2} d^{-1}, EP remains relatively low (85 mg C m^{-2} d^{-1}). Here EP accounts for only about 4 % of PP (see green data points in Fig. 4), suggesting that phytoplankton biomass was accumulating in the surface waters without significant export yet. In contrast, during KEOPS 1 (summer), EP fluxes reached 250 mgC m^{-2} d^{-1} at 125 m (14–31 % of PP) while PP ranged from 865 to 1872 mg C m^{-2} d^{-1}, reflecting enhanced export to the bottom (Blain et al., 2007; Jacquet et al., 2008a; Savoye et al., 2008).

In Fig. 5a we plot for both KEOPS cruises the ratio of EP over PP vs. the fraction of EP exported deeper than 400 m (i.e. T400; defined above). Note that for station A3-1 (KEOPS 2), there are no PP data. The A3 site shows increasing EP/PP ratios from spring (KEOPS 2) to late summer (KEOPS 1), and so do the T400 values (A3-1: 70 %; A3-2: 87 %; KEOPS 1 A3 site: 92 ± 1 %). Station E-4W located in waters with similar θ–S and Chl *a* characteristics as the A3 plateau site has PP and EP fluxes of the same order of magnitude (Table 2). However, MR values (36 mg C m^{-2} d^{-1}; 150–400 m) are larger at E-4W, resulting in a lower T400 value of around 33 %, compared to 87 % for A3-2 (Fig. 5a). When integrating down to 800 m, T800 at E-4W reaches 141 % (i.e., no export of POC beyond 800 m; note that > 100 % values, i.e., MR > EP, were set to zero in Fig. 5a). Station F-L (in the vicinity of the PF; 74.7° E) appears to function in a similar way as observed for E-4W (71.4° E). PP at station F-L is relatively high (3380 mg C m^{-2} d^{-1}), while EP is quite low (43 mg C m^{-2} d^{-1}), reflecting the fact that the biomass was not yet exported from the surface waters. Since MR fluxes are slightly lower (21 mg C m^{-2} d^{-1}; 150-400 m) at F-L than at E-4W, resulting T400 values are higher (52 %) there. Note that the particle flux at F-L was mainly composed of fecal pellet material while at A3 phytodetrital aggregates were dominant (Laurenceau et al., 2014).

Overall, it appears that biomass at stations A3, E-4W and F-L was accumulating in surface waters and export did not start yet considering the early stage of the season during KEOPS 2. Our observations allow us to conclude the following: (1) in contrast to A3, E-4W and F-L show important mesopelagic remineralization rates, reducing the

cc BY

efficiency of C sequestration beyond 800 m; (2) both seasons (KEOPS 1 and KEOPS 2) show a similar functioning of the mesopelagic ecosystem at A3. The rather low and perduring MR fluxes under high production and variable export regimes indicate that here mesopelagic remineralization is not a major resistance to organic matter transfer to the sea-floor at A3. On average (considering both seasons but excluding A3-1) the C sequestration efficiency into the deep (> 400 m) reached 91 ± 3 % at A3.

4.3 Stations in the meander

Here we will discuss temporal changes for the stations TNS-6, E-1, E-2, E-3, E-4E and E-5, located in the Polar front Meander, and which constitute a time series over the one month duration of this study. Note that no PP or EP data exist for TNS-6. From Table 2 it appears that the near doubling of the PP between E-1 and E-5 is not paralleled by an increase of EP and MR, except for the 30 % EP increase from E-1 to E-3. In fact overall EP shows a decreasing trend with time, while MR (150–400 m) stays rather constant, except for the decrease between E-1 and E-3 (Table 2). As reported above such a mismatch may result from differences in time scales characterizing the different processes that are compared. The more likely explanation, however, is that in this early stage of the growth season, phytoplankton biomass is accumulating in the surface layer and export is lagging behind.

The ratio of EP over PP vs. T400 and T800 reveals a large variability in sequestration efficiency inside the meander (Fig. 5b). PP and EP fluxes increase by about 30 % from E-1 to E-3, but a concomitant decrease of mesopelagic MR yields to an enhanced transfer efficiency, from 74 to 92 %, through the 400 m boundary and from 52 to 73 % through the 800 m boundary. This suggests that significant remineralization should also occur at greater depth (even at depths > 1000 m) as reflected also by the presence of Ba_{xs} maxima below 1000 m (see Table 1A). This becomes particularly salient when plotting Ba_{xs} contents vs. depths over the 27 day observation period (Fig. 5b). The high deep water Ba_{xs} values in Fig. 5b are not taken into account when integrating TNS-6 and E-1 profiles between 150 and 400 or even 150 and 800 m. Considering

BGD
11, 9035–9069, 2014

CC BY

that the seafloor in the meander area is at about 2000 m depth, it seems unlikely that these high Ba_{xs} contents at depths > 1000 m are due to sediment resuspension. Also, particle spectra for these sites do not reveal any bottom resuspension (Jouandet et al., 2014; Lasbleiz et al., 2014; Vandermerve et al., 2014; Zhou et al., 2014). Therefore, the high deep (> 1000 m) Ba_{xs} contents at TNS-6 and E-1 likely reflect the fact that here significant remineralization of POC material did occur in the bathypelagic domain and even down to the sea-floor. Note that suspended particles in the depth range containing the deep Ba_{xs} maxima were dominated by the < 2 µm size fraction (Zhou et al., 2014). When integrating the Ba_{xs} contents from 150 m till the sea-floor at stations TNS-6 and E-1, MR fluxes increase to 156 and 184 mg C m^{-2} d^{-1}, respectively. Such C fluxes are similar to the EP values (maximum value of 130 mg C m^{-2} d^{-1} at E-3) and suggest that exported POC is entirely remineralized in the water column leaving no C for sequestration into the sediments.

Overall, the temporal pattern of mesopelagic remineralization described above reflects two successive events of particle transfer: a first transfer from a past bloom (occurred before visiting TNS-6 and perduring at E-1) and a second transfer from E-4E to E-5. The first transfer is evident by the downward (up to the bottom) propagation of the mesopelagic Ba_{xs} maximum signal, which mostly weakens at E-2 (Fig. 5b). The second event is reflected by the occurrence again of important mesopelagic Ba_{xs} build-up at E-4E and E-5. Note that the particle flux composition in the meander shows a shift from a domination of fecal pellet to phytodetrital material from E-1 to E-3, and fecal pellets becoming more important again at E-5 (Laurenceau et al., 2014). Overall, our results indicate the large capacity of the Polar Front Meander to transfer POC material to depth, but in contrast to station A3 on the Plateau, this transfer is coupled to intense and near to complete POC remineralization (as also observed at E-4W and F-L). Between-sites changes in mesopelagic carbon remineralization due to unequal biomass productivity and iron fertilization over the Kerguelen Plateau are thus relatively complex. Furthermore, the situation in the Meander area seems to corroborate results obtained in the iron-replete Subantarctic Zone east of the Tasman Plateau (Australian

BGD
11, 9035–9069, 2014

cc BY

sector of the Southern Ocean; SAZ-Sense cruise; Jacquet et al., 2011), where the mesopelagic remineralization efficiency was reported relatively high (on average 91 %) and the deep (> 600 m) carbon sequestration weak (< 10 %).

5 Conclusion

Based on spatially and temporally well resolved mesopelagic excess particulate Ba inventories this work estimated mesopelagic POC remineralization above the Kerguelen Plateau and inside a permanent meander of the Polar Front to the east of Plateau, areas. The observed variability of mesopelagic remineralization reflects differences in the fate of the biomass that is exported to the deep ocean, between Plateau and Polar Front. In terms of deep ocean carbon sequestration efficiency, our results highlight that above the plateau (A3 site) mesopelagic remineralization is not a major barrier to organic matter transfer to the sea-floor, with carbon sequestration beyond 400 m reaching up to 87 % of EP, while in the Polar Front Meander remineralization of exported organic carbon in the upper 400 m is more efficient than above the plateau. In the Meander area remineralization may even balance export when including its effect in the deeper waters (till 800 m and even deeper), thus resulting in a close to zero carbon sequestration to sediment. A similar condition is observed for sites at the margin of the plateau (E-4W) and the Polar front (F-L).

Acknowledgements. We thank the officers and crew of R/V *Marion Dufresne* for their assistance during work at sea. We are indebted to chief scientist S. Blain and voyage leader B. Quéguiner for skillful leadership during the cruise and to the CTD team for managing rosette operation and CTD data. This research was supported by the French Agency of National Research grant (project KEOPS 2, #ANR-10-BLAN-0614), the Belgian Science Policy (BELSPO) project "BIGSOUTH" (SD/CA/05A), Flanders Research Foundation (FWO Project G071512N), the European Union Seventh Framework Programme (Marie Curie CIG "MuSiCC" under grant agreement no. 294146 to D.C.) and the Strategic Research Programme at Vrije Universiteit Brussel.

BGD
11, 9035–9069, 2014

References

Armand, L. K., Crosta, X., Quéguiner, B., Mosseri, J., and Garcia, N.: Diatoms preserved in surface sediments of the northeastern Kerguelen Plateau, Deep-Sea Res. Pt. II, 55, 677–692, 2008.

de Baar, H. J. W., Boyd, P. W., Coale, K. H., Landry, M. R., Tsud, A., Assmy, P., Bakker, D. C. E, Bozec, Y., Barber, R. T., Brzezinski, M. A., Buesseler, K. O., Boyé, M., Croot, P. L., Gervais, F., Gorbunov, Y., Harrison, P. J., Hiscock, W. T., Laan, P., Lancelot, C., Law, C.S., Levasseur, M., Marchetti, A., Millero, F. J., Nishika, J., Nojiri, Y., van Oijen, T., Riebesell, U., Rijkenberg, M. J. A., Saito, H., Takeda, S., Timmermans, K. R., Veldhuis, J. W., Waite, A. M., and Wong, C. S.: Synthesis of iron fertilization experiments: from the Iron Age in the Age of Enlightenment, J. Geophys. Res, 110, C09S16, doi:10.1029/2004JC002601, 2005.

Blain, S., Tréguer, P., Belviso, S., Bucciarelli, E., Denis, M., Desabre, S., Fiala, M., Martin Jézéquel, V., Le Fèvre, J., Mayzaud, P., Marty, J.-C., and Razouls, S.: A biogeochemical study of the island mass effect in the context of the iron hypothesis: Kerguelen Islands, Southern Ocean, Deep-Sea Res. Pt. I, 48, 163–187, 2001.

Blain, S., Queguiner, B., Armand, L., Belviso, S., Bombled, B., Bopp, L., Bowie, A., Brunet, C., Brussaard, C., Carlotti, F., Christaki, U., Corbiere, A., Durand, I., Ebersbach, F., Fuda, J.-L., Garcia, N., Gerringa, L., Griffiths, B., Guigue, C., Guillerm, C., Jacquet, S., Jeandel, C., Laan, P., Lefevre, D., Lo Monaco, C., Malits, A., Mosseri, J., Obernosterer, I., Park, Y.-H., Picheral, M., Pondaven, P., Remenyi, T., Sandroni, V., Sarthou, G., Savoye, N., Scouarnec, L., Souhaut, M., Thuiller, D., Timmermans, K., Trull, T., Uitz, J., van Beek, P., Veldhuis, M., Vincent, D., Viollier, E., Vong, L., and Wagener, T.: Effect of natural iron fertilization on carbon sequestration in the Southern Ocean, Nature, 446, 1070–1074, 2007.

Blain, S., Quéguiner, B., and Trull, T.: The natural iron fertilization experiment KEOPS (KErguelen Ocean and Plateau compared Study): an overview, Deep-Sea Res. Pt. II, 55, 559–565, 2008.

Boyd, P. W., Watson, A. J., Law, C. S., Abraham, E. R., Trull, T., Murdoch, R., Bakker, D. C. E., Bowie, A. R., Buesseler, K. O., Chang, H., Charette, M., Croot, P., Downing, K., Frew, R., Gall, M., Hadfield, M., Hall, J., Harvey, M., Jameson, G., LaRoche, J., Liddicoat, M., Ling, R., Maldonado, M. T., McKay, R. M., Nobber, S., Pickmere, S., Pridmore, R., Rintoul, S., Safi, K., Sutton, P., Strzepek, R., Tanneberger, K., Turner, S., Waite, A., and Zeldis, J.: Phytoplankton

CC BY

bloom upon mesoscale iron fertilisation of polar Southern Ocean waters, Nature, 407, 695–702, 2000.
Boyd, P. W., Law, C. S., Wong, C. S., Nojiri, Y., Tsuda, A., Levasseur, M., Takeda, S., Rivkin, R., Harrison, P. J., Strzepek, R., Gower, J., McKay, R. M., Abraham, E., Arychuk, M., Barwell-Clarke, J., Crawford, W., Crawford, D., Hale, M., Harada, K., Johnson, K., Kiyosawa, H., Kudo, I., Marchetti, A., Miller, W., Needoba, J., Nishioka, J., Ogawa, H., Page, J., Robert, M., Saito, H., Sastri, A., Sherry, N., Soutar, T., Sutherland, N., Taira, Y., Whitney, F., Wong, S. K. E., and Yoshimura, T.: The decline and fate of an iron-induced subarctic phytoplankton bloom, Nature, 428, 549–553, 2004.
Bowie, A. R., et al.: Iron budgets for trhee distrinct biogeochemical sites around the Kerguenlen plateau (Southern Ocean) during the natural fertilization experiment KEOPS2, submitted, this issue, 2014.
Broecker, W. S., Takahashi, T., and Takahashi, T.: Sources and flow patterns of deep-ocean waters as deduced from potential temperature, salinity and initial phosphate concentration, J. Geophys. Res., 90, 6925–6939, 1985.
Buesseler, K. O. and Boyd, P. W.: Shedding light on processes that control particle export and flux attenuation in the twilight zone, Limnol. Oceanogr., 54, 1210–1232, 2009.
Buesseler, K. O., Andrews, J. E., Pike, S. M., and Charette, M. A.: The effect of iron fertilization on carbon sequestration in the Southern Ocean, Science, 304, 414–417, 2004.
Buesseler, K. O., Andrews, J. E., Pike, S. M., Charette, M. A., Goldson, L. E., Brzezinski, M. A., and Lance, V. P.: Particle export during the Southern Ocean Iron Experiment (SOFeX), Limnol. Oceanogr., 50, 311–327, 2005.
Buesseler, K. O., Lamborg, C. H., Boyd, P. W., Lam, P. J., Trull, T. W., Bidigare, R. R., Bishop, J. K. B., K. L., Casciotti, Dehairs, F., Elskens, M., Honda, M., Karl, D. M., Siegel, D. A., Silver, M. W., Steinberg, D. K., Valdes, J., Van Mooy, B., and Wilson, S.: Revisiting carbon flux through the ocean's twilight zone, Science, 316, 567–569, 2007.
Cardinal, D., Dehairs, F., Cattaldo, T., and André, L.: Constraints on export and advection in the Subantarctic and Polar Front Zones, south of Australia from the geochemistry of suspended particles, J. Geophys. Res.-Oceans, 106, 31637–31656, doi:10.1029/2000JC000251, 2001.
Cardinal, D., Savoye, N., Trull., T. W., André, L., Kopczynska, E., and Dehairs, F.: Particulate Ba distributions and fluxes suggest latitudinal variations of carbon mineralization in the Southern ocean, Deep-Sea Res. Pt. I, 52, 355–370, 2005.

CC BY

Cavagna, A. J., et al.: Biological productivity regime and in-situ methods comparison around the Kerguelen Island in the Southern Ocean, submitted, this issue, 2014.
Dehairs, F., Chesselet, R., and Jedwab, J.: Discrete suspended particles of barite and the barium cycle in the open ocean, Earth Planet. Sc. Lett., 49, 40–42, 1980.
Dehairs, F., Baeyens, W., and Goeyens, L.: Accumulation of suspended barite at mesopelagic depths and export production in the Southern Ocean, Science, 258, 1332–1335, 1992.
Dehairs, F., Shopova, D., Ober, S., Veth, C., and Goeyens, L.: Particulate barium stocks and oxygen consumption in the Southern Ocean mesopelagic water column during spring and early summer: relationship with export production, Deep-Sea Res. Pt II, 44, 497–516, 1997.
Dehairs, F., Jacquet, S. H. M., Savoye, N., van Mooy, B., Buesseler, K., Bishop, J., Lamborg, C., Elskens, M., Baeyens, W., Casciotti, K., and Monnin, C.: Barium in twilight zone suspended matter as proxy for organic carbon mineralization: results for the North Pacific, Deep-Sea Res. Pt. II, 55, 1673–1683, 2008.
Dehairs, F., et al.: Nitrate isotopic composition in the Kerguelen area (Southern Ocean) during KEOPS2, submitted, this issue, 2014.
D'ovidio, F., et al.: Pathway of iron dispersion off Kergueln plateau: the role of horizontal stirring, submitted, this issue, 2014.
Dymond, J. R., Suess, E., and Lyle, M.: Barium in deep-sea sediment: a geochemical proxy for paleoproductivity, Paleoceanography, 7, 163–181, 1992.
Ellison, S. L. R.: Eurachem/CITAC Guide CG4, Quantifying Uncertainty in Analytical Measurement, 2nd edn., edited by: Ellison, S. L. R., Rosslein, M., and Williams, A., 120 pp., 2000.
François, R., Honjo, S., Krishfield, R., and Manganini, S.: Factors controlling the flux of organic carbon to the bathypelagic zone of the ocean, Global Biogeochem. Cy., 16, 1087, doi:10.1029/2001GB001722, 2002.
Gervais, F., Riebesell, U., and Gorbunov, M. Y.: Changes in primary productivity and chlorophyll a in response to iron fertilization in the southern Polar Frontal Zone, Limnol. Oceanogr., 47, 1324–1335, 2002.
Hoffmann, L., Peeken, I., Lochte, K., Assmy, P., and Veldhuis, M.: Different reactions of Southern Ocean phytoplankton size classes to iron fertilization, Limnol. Oceanogr., 51, 1217–1229, 2006.
Jacquet, S. H. M., Dehairs, F., Cardinal, D., Navez, J., and Delille, B.: Barium distribution across the Southern Ocean Frontal system in the Crozet-Kerguelen Basin, Mar. Chem., 95, 149–162, 2005.

BGD
11, 9035–9069, 2014

Early season mesopelagic C remineralization and transfer efficiency

S. H. M. Jacquet et al.

CC BY

Jacquet, S. H. M., Dehairs, F., Elskens, M., Savoye, N., and Cardinal, D.: Barium cycling along WOCE SR3 line in the Southern Ocean, Mar. Chem., 106, 33–45, 2007.

Jacquet, S. H. M., Dehairs, F., Savoye, N., Obernosterer, I., Christaki, U., Monnin, C., and Cardinal, D.: Mesopelagic organic carbon mineralization in the Kerguelen Plateau region tracked by biogenic particulate Ba, Deep-Sea Res. Pt. II, 55, 868–879, 2008a.

Jacquet, S. H. M., Savoye, N., Dehairs, F., Strass, V., and Cardinal, D.: Mesopelagic carbon mineralization during the European Iron Fertilization Experiment (EIFEX), Glob. Biogeochem. Cy., 22, GB1023, doi:10.1029/2006GB002902, 2008b.

Jacquet, S. H. M., Dehairs, F., Becquevort, S., Dumont, I., Cavagna, A., and Cardinal, D.: Twilight zone organic carbon remineralization in the PFZ and SAZ south of Tasmania (Southern Ocean), Deep-Sea Res. Pt. II, 58, 2222–2234, doi:10.1016/j.dsr2.2011.05.029, 2011a.

Jacquet, S. H. M., Lam, P., Trull, T., and Dehairs, F.: Carbon export production in the Polar front zone and Subantarctic Zone south of Tasmania, Deep-Sea Res. Pt. II, 58, 2277–2292, doi:10.1016/j.dsr2.2011.05.035, 2011b.

Jouandet, M. P., et al.: Particles distribution in contrasted area of the iron fertilized region around Kerguenlen Islans, in preparation, this issue, 2014.

Lampitt, R. S. and Antia, A. N.: Particle flux in deep seas: regional characteristics and temporal variability, Deep-Sea Res. Pt. I, 44, 1377–1403, 1997.

Lasbleiz, M., et al.: Particulate matter distribution in relation to phytoplakton community structure in the Fe-fertilized Kergueln region of the SOuthern Ocean during austral spring (KEOPS2), submitted, this issue, 2014.

Laurenceau, E., et al.: The relative importance of phytodetrital aggregates and fecal pellets in the control of export fluxes from naturally iron-fertilised waters near the Kerguelen plateau, submitted, this issue, 2014.

Lefèvre, D., Guigue, C., and Obernosterer, I.: The metabolic balance at two contrasting sites in the Southern Ocean: the iron-fertilized Kerguelen area and HNLC waters, Deep-Sea Res. Pt. II, 55, 766–776, doi:10.1016/j.dsr2.2007.12.006, 2008.

Longhurst, A. R., Bedo, A. W., Harrison, W. G., Head, E. J. H., and Sameoto, D. D.: Vertical flux of respiratory carbon by oceanic diel migrant biota, Deep-Sea Res., 37, 685–694, 1990.

Martin, J. H., Knauer, G. A., Karl, D. M., and Broenkow, W. W.: VERTEX: carbon cycling in the NE Pacific, Deep-Sea Res., 34, 267–285, 1987.

Monnin, C., Jeandel, C., Cattaldo, T., and Dehairs, F.: The marine barite saturation state of the world's oceans, Mar. Chem., 65, 253–261, 1999.

BGD
11, 9035–9069, 2014

Early season mesopelagic C remineralization and transfer efficiency

S. H. M. Jacquet et al.

CC BY

Morris, P. J. and Charette, M. A.: A synthesis of upper oceancarbon and dissolved iron budgets for Southern Ocean natural iron fertilization studies, Deep-Sea Res., 90, 147–157, 2013.
Mosseri, J., Quéguiner, B., Armand, L. K., and Cornet-Barthaux, V.: Impact of iron on silicon utilization by diatoms in the Southern Ocean: a case study of Si/N cycle decoupling in a naturally iron-enriched area, Deep-Sea Res. Pt. II, 55, 801–819, doi:10.1016/j.dsr2.2007.12.003, 2008.
Park, Y., et al.: Water masses and criculation in the Poalr Front region east of the Kerguelen Islands, submitted, this issue, 2014.
Planchon, F., Cavagna, A.-J., Cardinal, D., André, L., and Dehairs, F.: Late summer particulate organic carbon export and twilight zone remineralisation in the Atlantic sector of the Southern Ocean, Biogeosciences, 10, 803–820, doi:10.5194/bg-10-803-2013, 2013.
Planchon, F., et al.: Carbon export in the naturally iron-fertilized Kerguelen area of the Southern Ocean using 234Th-based approach, in preparation, this issue, 2014.
Pollard, R. T., Salter, I., Sandars, R. J., Lucas, M. I., Mark Moore, C., Mills, R. A., Statham, P. J., Allen, J. T., Baker, A. R., Bakker, C. E., Charrette, M. A., fielding, S., Fones, G. R., French, M., Hickman, A. E., Holland, R. J., Hughes, J. A., Jickells, T. D., Lampitt, R. S., Morris, P. J., Nédélec, F. H., Nielsdottir, M., Planquette, H., Popova, E. E., Poulton, A. J., Read, J. F., Seeyave, S., Smith, T., Stinchcombe, M., Taylor, S., Thomalla, S., Venables, H. J., Williamson, R., and Zubkov., M.: Southern Ocean deep-water carbon export enhanced by natural iron fertilization, Nature, 457, 577–580, doi:10.1038/nature07716, 2009.
Ridgway, K. R. and Dunn, J. R.: Observational evidence for a Southern Hemisphere oceanic supergyre, Geophy. Res. Lett, 34, L13612, doi:10.1029/2007GL030392, 2007.
Salter, I., Lampitt, R. S., Sanders, R., Poulton, A., Kemp, A. E. S., Boorman, B., Saw, K., and Pearce, R.: Estimating carbon, silica and diatom export from a naturally fertilised phytoplankton bloom in the Southern Ocean using PELAGRA: a novel drifting sediment trap, Deep-Sea Res. Pt. II, 54, 2233–2259, 2007.
Sarmiento, J. L., Slater, R. D., Fasham, M. J. R., Ducklow, H. W., and Toggweiler, J. R.: A seasonal three-dimensional ecosystem model of nitrogen cycling in the North Atlantic photic zone, Global Biogeochem. Cy., 7, 417–450, 1993.
Savoye, N., Trull, T., Jacquet, S. H. M., Navez, J., and Dehairs, F.: ^{234}Th-derived export fluxes during a natural iron fertilization experiment (KEOPS), Deep-Sea Res. Pt. II, 55, 841–855, 2008.
Schlitzer, R.: Ocean Data View, available at: http://www.awi-bremerhaven.de/GEO/ODV, 2002.

BGD
11, 9035–9069, 2014

CC BY

Schneider, B., Bopp, L., and Gehlen, M.: Assessing the sensitivity of modeled airsea CO_2 exchange to the remineralization depth of particulate organic and inorganic carbon, Global Biogeochem. Cy., 22, GB3021, doi:10.1029/2007GB003100, 2008.

Shopova, D., Dehairs, F., and Baeyens, W.: A simple model of biogeochemical element distribution in the oceanic water column, J. Marine Syst., 6, 331–344, 1995.

Smetacek, V., Klass, C., Strass, V. H., Assmy, P., Montresor, M., Cisewki, B., Savoye, N., Webb, A., d'Ovidio, F., Arrieta, J. M., Bathmann, U., Bellerby, R., Mine Berg, G., Croot, P., Gonzalez, S., Jenjes, J., Herndl, G.J., Hoffmann, L.J., Leach, H., Losh, M., Mills, M. M., Neill, C., Peeken, I., Rottgers, R., Sachs, O., Sauter, E., Schmidt, M. M., Schwarz, J., Terbruggen, A., amd Wolf-Gladrow, D.: Deep carbon export from a Southern Ocean iron-fertilized diatom bloom, Nature, 487, 313–319, doi:10.1038/nature11229, 2012.

Strass, V., Cisewski, B., Gonzales, S., Leach, H., Loquay, K.-D., Prandke, H., Rohr, H., and Thomas, M.: The physical setting of the European Iron Fertilization Experiment "EIFEX" in the Southern Ocean, Reports on Polar and Marine Research, 500, 15–49, 2005.

Stroobants, N., Dehairs, F., Goeyens, L., Vanderheijden, N., and Van Grieken, R.: Barite formation in the Southern Ocean water column, Mar. Chem., 35, 411–422, 1991.

Taylor, S. R. and McLennan, S. M.: The Continental Crust: its Composition and Evolution, Blackwell Scientific Publications, 312 pp., 1985.

Trull, T., et al.: Phytoplankton size and compositions variations in naturally iron fertilised Southern Ocean waters: evidence for differing propensities for carbon export in waters dowstrem versus over the Kerguelen plateau, in preparation, this issue, 2014.

Vandermerve, P., et al.: Sourcing the iron in the naturally-fertilised bloom around the Kerguelen plateau: particulate trace metal dynamics, submitted, this issue, 2014.

Venchiarutti, C., Jeandel, C., and Roy-Barman, M.: Particle dynamics study in the wake of Kerguelen Island using thorium isotopes, Deep-Sea Res. Pt. I, 55, 1343–1363, 2008.

Zhou, M., Zhu, Y., Dorland, R. D., and Measures, C. I.: Dynamics of the current system in the southern Drake Passage, Deep-Sea Res. Pt. I, 57, 1039–1048, 2010.

Zhou, M., Zhu, Y., Measures, C. I., Hatta, M., Charette, M. A., Gille, S. T., Frants, M., Jiang, M., and Mitchell, B. G.: Winter mesoscale circulation on the shelf slope region of the southern Drake Passage, Deep-Sea Res. Pt. II, 90, 4–14, 2013.

Zhou, M., et al.: Estimates of particle settling and scavenging using LISST-LOPC in Kergueln Plateau regions during the 2011 austral spring KEOPS II cruise, submitted, this issue, 2014.

BGD

11, 9035–9069, 2014

Early season mesopelagic C remineralization and transfer efficiency

S. H. M. Jacquet et al.

CC BY

Table 1. Station locations, casts number and bottom depth during KEOPS 2. Depth-weighted average values (DWAv) of mesopelagic Ba_{xs} (pM) and Ba_{xs} based mesopelagic POC remineralization (MR; mg C m^{-2} d^{-1}) integrated between 150–400 and 150–800 m depths. See text for further information on calculation.

Station	CTD cast #	Long (° E)	Lat (° S)	Date of sampling	Seafloor [m]	DWAv[b] Ba_{xs}[pM] 150–400 m	DWAv Ba_{xs}[pM] 150–800 m	MR[c] 150–400 m [mg C m^{-2} d^{-1}]	MR Stnd Uncertainty %	MR 150–800 m [mg C m^{-2} d^{-1}]	MR Stnd Uncertainty %
Plateau											
A3-1	4[a]	72.080	50.629	20 Oct 2011	530	316	/	14	4	/	/
A3-2	107[a]	72.056	50.624	16 Nov 2011	527	267	/	11	5	/	/
TEW-3	38	71.018	48.799	31 Oct 2011	560	324	/	28	8	/	/
Meander time series											
TNS-6	10	72.277	48.779	22 Oct 2011	1885	427	389	31	7	69	17
E-1	27/30	72.187	48.458	29, 30 Oct 2011	2056	387	325	26	6	48	14
E-2	43	72.077	48.523	1 Nov 2011	2003	301	309	15	5	42	13
E-3	50/55	71.967	48.702	3, 4 Nov 2011	1915	258	286	10	4	35	12
E-4E	94/97	72.563	48.715	13, 14 Nov 2011	2210	395	357	27	7	58	15
E-5	113/114	71.900	48.412	18 Nov 2011	1920	402	380	28	7	66	17
Polar Front Zone											
TNS-1	15	71.501	46.833	23 Oct 2011	2280	350	315	22	6	45	14
TEW-8	47	74.999	48.471	2 Nov 2011	2786	199	240	2	4	20	11
F-L	63/68	74.659	48.532	6, 7 Nov 2011	2695	345	328	21	6	49	14
Polar Front											
E-4W	81/87	71.425	48.765	11, 12 Nov 2011	1384	468	411	36	8	76	18
Antarctic Zone											
R-2 (Reference site)	17/20	66.717	50.359	25, 26 Oct 2011	2300	572	456	50	10	91	20
TNS-8	8	72.240	49.463	21 Oct 2011	1030	473	358	37	8	59	15

[a] Station A3 (CTD #4 and #107); integration up to 354 and 405 m.
WAV[b] = Depth weighted average value.
MR[c] = Mesopelagic C remineralization.

BGD
11, 9035–9069, 2014

Early season mesopelagic C remineralization and transfer efficiency

S. H. M. Jacquet et al.

CC BY

Table 2. Comparison of mesopelagic POC remineralization (MR) with primary production (PP) and export production (EP). All fluxes in $mg\,C\,m^{-2}\,d^{-1}$. *r* ratio is the ratio of Mr over EP. The C sequestration (or transfer) efficiency at 400 and 800 m (T400, T800) is the fraction of C export (EP) at 150 m exiting through the 400 m (T400) or the 800 m (T800) horizons. See text for further information on calculation.

Station	CTD	MLD [m]	Ez[b] [m]	PP[c] Ez [$mg\,C\,m^{-2}\,d^{-1}$]	EP[d] 150 m [$mg\,C\,m^{-2}\,d^{-1}$]	MR 150–400 m [$mg\,C\,m^{-2}\,d^{-1}$]	MR 150–800 m [$mg\,C\,m^{-2}\,d^{-1}$]	EP/PP	*r* ratio 150–400 m	*r* ratio 150–800 m	T400	T800
Plateau												
A3-1	4[a]	161	/	/	47	14	/	/	0.29	/	0.70	/
A3-2	107[a]	165	38	2172	85	11	/	0.04	0.13	/	0.87	/
Reference site												
R-2	17/20	111	92	132	30	50	91	0.23	1.65	3.02	1.65	3.02
Meander time series												
E-1	27/30	84	64	578	100	26	48	0.17	0.26	0.48	0.74	0.52
E-3	50/55	41	68	748	130	10	35	0.17	0.08	0.27	0.92	0.73
E-4E	94/97	77	34	1037	48	27	58	0.05	0.57	1.21	0.43	1.21
E-5	113/114	36	54	1064	84	28	66	0.08	0.33	0.78	0.67	0.22
Polar Front Zone												
F-L	63/68	21	29	3380	43	21	49	0.01	0.48	1.13	0.52	1.13
Polar Front												
E-4W	81/87	67	31	3287	54	36	76	0.02	0.67	1.41	0.33	1.41

[a] Station A3 (CTD4 and 107); MR integrated up to 354 and 405 m.
[b] EZ euphotic layer (till 1 % PAR level).
[c] PP data from Cavagna et al. (2014).
[d] EP data from PLanchon et al. (2014).

BGD
11, 9035–9069, 2014

Table A1. Excess particulate biogenic Ba (Ba_{xs}; pM) and particulate Al (nM) during KEOPS 2.

Station A3								Station RK2							
A3-1 CTD4				A3-2 CTD 107				R-2 CTD17				R-2 CTD 20			
Niskin	Depth [m]	Ba_{xs} [pM]	Al [nM]	Niskin	Depth [m]	Ba_{xs} [pM]	Al [nM]	Niskin	Depth [m]	Ba_{xs} [pM]	Al [nM]	Niskin	Depth [m]	Ba_{xs} [pM]	Al [nM]
23	11	224	35	23	11	122	16	24	21	110	107	17	356	546	12
21	42	217	64	21	40	140	12	23	40	0	693	15	507	239	17
19	104	345	65	19	81	141	10	22	80	95	49	13	609	226	7
17	152	234	19	17	126	82	27	20	100	131	27	11	812	267	3
15	173	244	19	15	151	119	14	18	126	168	5	10	1011	189	2
13	204	333	17	13	176	199	9	16	151	205	4	8	1520	201	4
11	227	235	8	11	202	186	14	14	203	334	3	6	1832	184	2
9	253	315	6	9	277	323	24	13	253	616	6	1	2473	286	3
7	279	480	8	7	303	359	32	12	304	834	16				
5	354	216	21	5	405	247	19	10	404	573	9				
1	474	1108	155	1	513	1842	186	9	507	430	10				
								7	608	367	4				
								5	708	337	10				
								1	911	368	13				

Station E															
E-1 CTD 27				E-1 CTD 30				E-2 CTD 43				E-3 CTD 50			
Niskin	Depth [m]	Ba_{xs} [pM]	Al [nM]	Niskin	Depth [m]	Ba_{xs} [pM]	Al [nM]	Niskin	Depth [m]	Ba_{xs} [pM]	Al [nM]	Niskin	Depth [m]	Ba_{xs} [pM]	Al [nM]
24	21	896	166	17	303	424	30	23	11	192	43	24	11	129	45
23	41	221	131	16	353	195	25	21	41	93	152	23	42	117	93
22	81	190	161	15	455	143	6	18	102	143	17	22	71	130	28
20	101	172	102	13	505	268	6	16	153	215	57	20	102	160	22
18	125	150	10	11	636	343	7	14	204	408	9	18	125	201	11
16	151	290	9	10	808	138	2	12	254	311	6	16	153	225	18
14	182	375	5	8	1011	442	4	10	305	227	4	14	203	193	3
13	253	450	12	6	1498	436	9	8	406	353	5	13	252	210	2
12	303	402	9	1	2042	326	7	7	507	371	9	12	304	309	6
10	403	327	10					6	609	271	10	10	404	316	7
9	505	230	6					5	813	297	14	9	505	419	64
7	605	305	10					4	1016	350	35	7	606	320	14
5	707	298	10					1	2020	302	11	5	707	193	12
1	913	309	7									1	912	265	5

cc BY

Table A1. Continued.

Station E (continued)

E-3 CTD 55				E-4W CTD 81				E-4W CTD 87				E-4E CTD 94			
Niskin	Depth [m]	Ba_{xs} [pM]	Al [nM]	Niskin	Depth [m]	Ba_{xs} [pM]	Al [nM]	Niskin	Depth [m]	Ba_{xs} [pM]	Al [nM]	Niskin	Depth [m]	Ba_{xs} [pM]	Al [nM]
17	404	185	5	24	10	101	16	17	304	277	9	24	20	116	32
16	455	272	5	23	41	134	17	16	354	350	10	23	51	260	11
15	505	176	6	22	70	152	5	15	453	233	7	22	93	563	223
13	605	378	5	20	94	86	18	13	606	182	9	20	103	170	5
11	810	258	3	18	126	84	7	11	811	186	5	18	126	215	9
10	910	172	2	16	153	193	8	10	910	187	7	16	152	210	6
8	1012	184	3	14	203	312	4	8	1011	268	61	14	181	247	7
6	1214	228	6	13	252	628	17	6	1214	249	29	13	253	547	4
1	1908	237	9	12	304	488	12	1	1384	250	30	12	305	403	78
				10	406	594	11					10	404	408	26
				9	507	272	11					9	505	403	26
				7	607	418	12					7	606	298	13
				5	708	338	21					5	706	285	8
				1	909	294	14					1	912	245	65

Station E (continued)

E-4E CTD 97				E-5 CTD 113				E-5 CTD 114			
Niskin	Depth [m]	Ba_{xs} [pM]	Al [nM]	Niskin	Depth [m]	Ba_{xs} [pM]	Al [nM]	Niskin	Depth [m]	Ba_{xs} [pM]	Al [nM]
21	404	199	2	10	911	111	3	24	11	210	5
18	505	242	3	8	1011	266	16	23	41	196	14
13	706	175	1	6	1214	256	15	22	82	245	4
8	1012	212	11	1	1922	208	5	20	102	264	14
7	1265	189	2					18	126	131	6
6	1518	149	2					16	152	153	5
5	1827	225	43					14	202	181	2
4	2027	212	12					13	252	469	6
1	2212	254	9					12	302	606	9
								10	404	377	13
								9	507	422	11
								7	606	425	7
								5	707	281	12
								1	910	281	6

BGD
11, 9035–9069, 2014

Early season mesopelagic C remineralization and transfer efficiency

S. H. M. Jacquet et al.

CC BY

Table A1. Continued.

Transect West–East								Station F-L							
TEW-3 CTD38				TEW-8 CTD 47				F-L CTD 63				F-L CTD 68			
Niskin	Depth [m]	Ba$_{xs}$ [pM]	Al [nM]	Niskin	Depth [m]	Ba$_{xs}$ [pM]	Al [nM]	Niskin	Depth [m]	Ba$_{xs}$ [pM]	Al [nM]	Niskin	Depth [m]	Ba$_{xs}$ [pM]	Al [nM]
23	16	133	40	23	10	196	31	24	11	146	37	17	405	264	6
21	41	107	112	21	41	0	251	23	35	97	41	16	456	233	9
19	61	209	45	18	102	92	41	22	61	0	228	15	506	339	12
17	76	148	20	16	152	169	45	20	82	141	36	13	607	265	3
13	112	128	13	14	202	134	9	18	101	134	5	11	910	718	7
11	183	235	8	12	254	164	5	16	126	185	5	10	1013	257	5
9	253	391	11	10	304	268	12	14	151	221	5	8	1215	316	8
7	277	348	9	8	405	217	5	13	202	280	7	6	1772	225	7
5	404	356	8	7	507	319	5	12	252	399	8	1	2741	2999	131
1	545	242	13	6	609	209	8	10	303	420	7				
				5	809	330	14	9	404	305	26				
				4	1011	334	22	7	506	408	7				
				1	2812	11179	826	5	707	247	10				
								1	911	282	11				

Transect North–South											
TNS-1 CTD15				TNS-6 CTD 10				TNS-8 CTD8			
Niskin	Depth [m]	Ba$_{xs}$ [pM]	Al [nM]	Niskin	Depth [m]	Ba$_{xs}$ [pM]	Al [nM]	Niskin	Depth [m]	Ba$_{xs}$ [pM]	Al [nM]
23	11	262	62	23	35	182	26	23	12	478	45
21	41	30	90	21	42	141	12	21	41	258	53
18	102	93	15	18	103	143	14	18	102	303	32
16	153	225	17	16	184	413	11	16	150	1008	33
14	202	289	5	14	204	461	8	14	205	341	10
12	253	228	2	12	255	298	5	12	254	447	6
10	304	521	4	10	306	505	7	10	305	481	4
8	405	346	3	8	407	474	4	8	405	312	3
7	506	230	1	7	509	464	9	7	505	208	3
6	607	352	13	6	610	315	15	6	606	283	7
5	809	234	4	5	813	269	9	5	707	325	11
4	1520	127	6	4	1526	362	13	4	910	376	35
1	2282	211	19	1	1886	410	21	1	1000	294	28

BGD
11, 9035–9069, 2014
Early season mesopelagic C remineralization and transfer efficiency
S. H. M. Jacquet et al.

CC BY

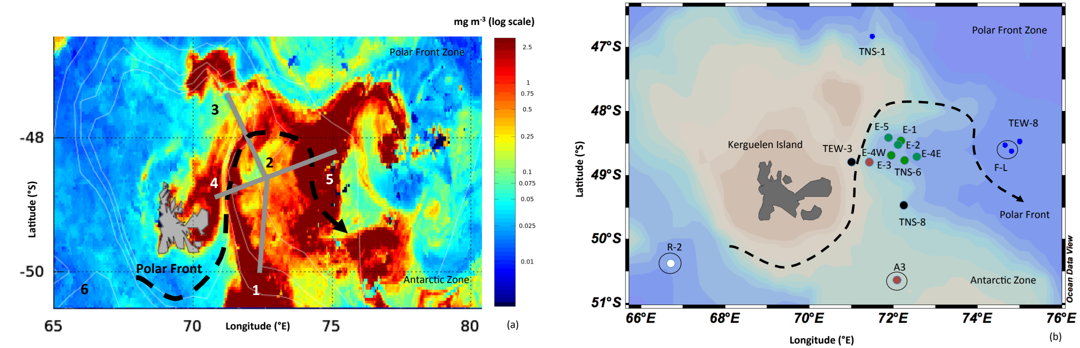

Figure 1. (a) Kerguelen Island area in the Southern Ocean with KEOPS 2 sampling zones and MODIS Chlorophyll concentrations (mg m^{-3}) (Chl *a* map from 11 November 2011, courtesy F. d'Ovidio) superposed. 1 refers to station A3, 2 to stations E, 3 to the North–South Transect, 4 to the West–East Transect, 5 to station F-L and 6 to reference station R-2; **(b)** corresponding stations location. Colors indicate stations with similar θ–S and Chl *a* characteristics.

BGD

11, 9035–9069, 2014

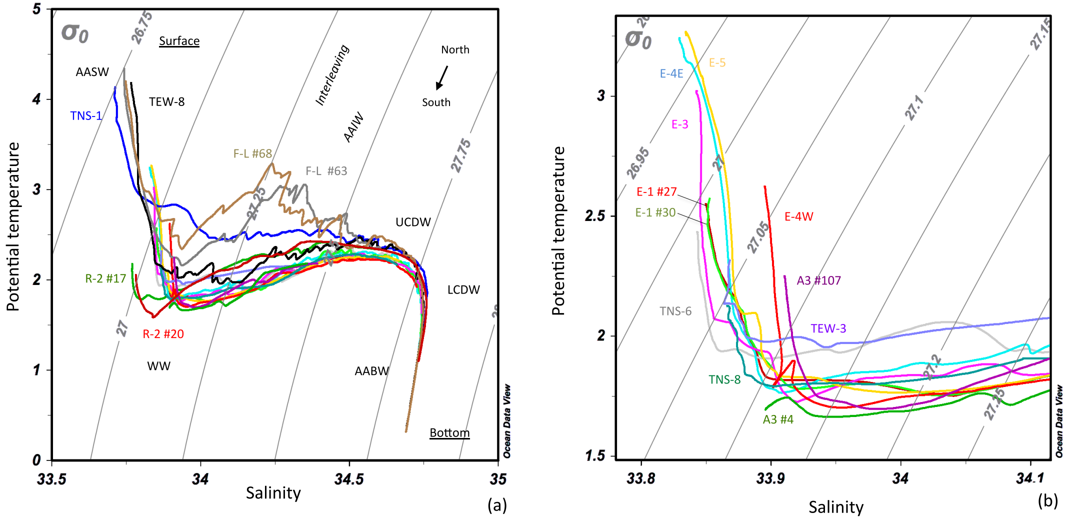

Figure 2. (a) Potential temperature θ–salinity S plots and isopycnals for KEOPS 2 profiles, **(b)** Focus on the upper 200 m water column. AASW = Antarctic Surface Waters, AAIW = Antarctic Intermediate Waters, WW = Winter Waters, UCDW and LCDW = Upper and Lower Circumpolar Deep Water, AABW = Antarctic Bottom Water. Graph constructed using Ocean Data View (Schlitzer, 2002; Ocean Data View; http://www.awi-bremerhaven.de/GEO/ODV).

BGD

11, 9035–9069, 2014

Early season mesopelagic C remineralization and transfer efficiency

S. H. M. Jacquet et al.

Title Page
Abstract | Introduction
Conclusions | References
Tables | Figures
Back | Close
Full Screen / Esc
Printer-friendly Version
Interactive Discussion

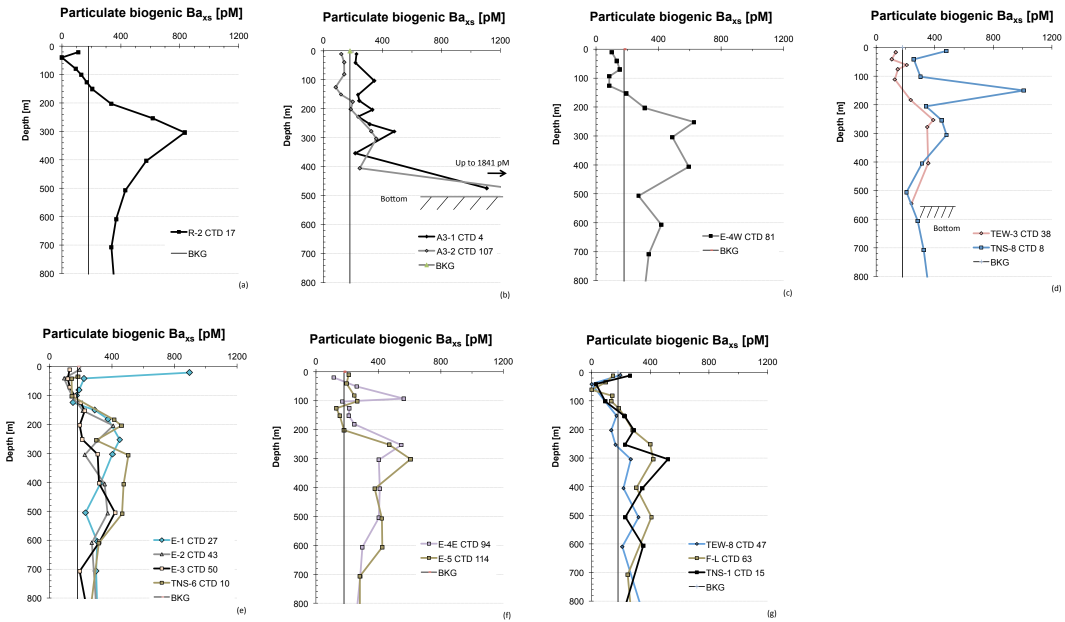

Figure 3. Particulate biogenic Ba$_{xs}$ profiles (pM) in the upper 800 m. Station identified by the CTD cast numbers. BKG = Ba$_{xs}$ background (180 pM).

BGD
11, 9035–9069, 2014

Early season mesopelagic C remineralization and transfer efficiency

S. H. M. Jacquet et al.

Title Page
Abstract | Introduction
Conclusions | References
Tables | Figures
◀| |▶
◀ ▶
Back | Close
Full Screen / Esc
Printer-friendly Version
Interactive Discussion

CC BY

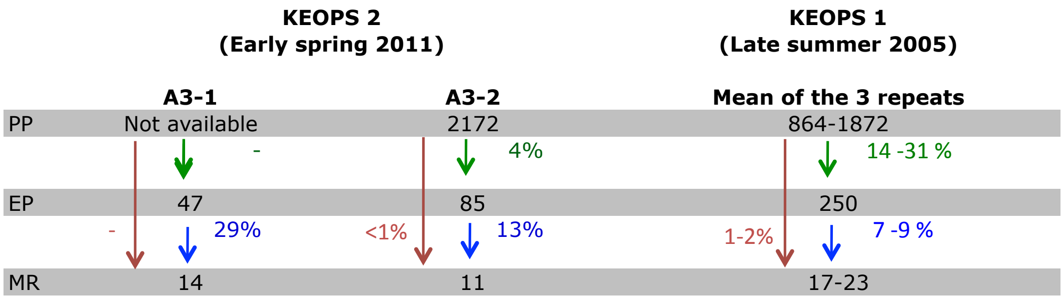

Figure 4. Schematic, comparing the fate of POC at station A3 during KEOPS 1 and KEOPS 2 cruises. PP = primary production, EP = export production at 150 m depth and MR = mesopelagic POC remineralization integrated between 150–400 m; all fluxes in $\mathrm{mg\,C\,m^{-2}\,d^{-1}}$. EP/PP (green values), MR/PP (red values) and MR/EP (r ratio, mesopelagic remineralization efficiency, blue values) ratios shown as %.

BGD
11, 9035–9069, 2014

BGD
11, 9035–9069, 2014

Early season mesopelagic C remineralization and transfer efficiency

S. H. M. Jacquet et al.

CC BY

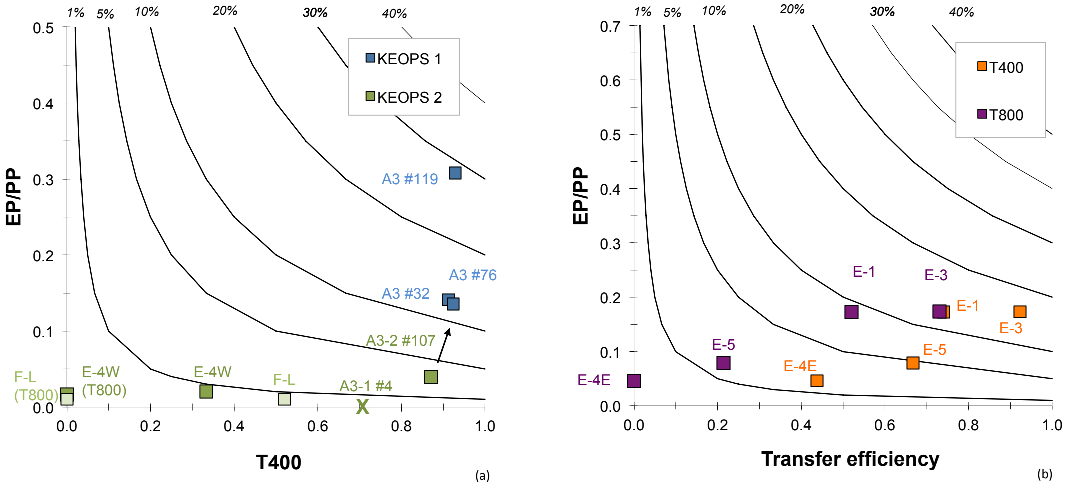

Figure 5. *y* axis: EP/PP = POC flux at 150 m (EP150) as a fraction of primary production (PP); *x* axis: EPx/EP150 = POC flux at defined depths (EPx; here 400 and 800 m) as a fraction of POC flux at 150 m (EP150). The green cross (Fig. 5a) is for station A3-1 (KEOPS-2). Since no PP data is available for this station, the EP/PP value has been arbitrarily set to 0. Isolines represent the modeled 1, 5, 10, 20 and 30 % of PP export to depths > at 400 or 800 m, and represent export efficiency.

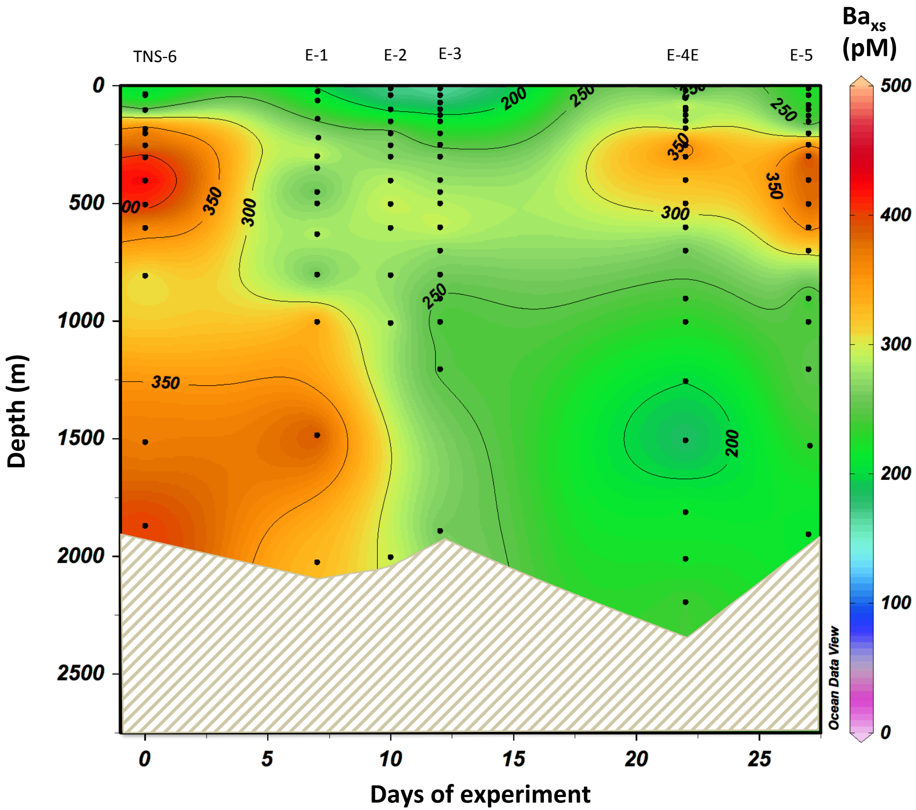

Figure 6. Temporal evolution in the meander of particulate biogenic Ba (Ba_{xs}; pM) in the upper 2000 m water column. Graph constructed using Ocean Data View (Schlitzer, 2002; Ocean Data View; http://www.awi-bremerhaven.de/GEO/ODV).

CC BY